High-Frame-Rate Contrast Echocardiography using diverging waves: initial in-vitro and in-vivo evaluation

High-Frame-Rate Contrast Echocardiography Using Diverging Waves: Initial *In Vitro* and *In Vivo* Evaluation

Matthieu Toulemonde, *Member, IEEE*, Yuanwei Li, Shengtao Lin, *Graduate Student Member, IEEE*, Fabien Cordonnier, Mairead Butler, W. Colin Duncan, Robert J. Eckersley, *Senior Member, IEEE*, Vassilis Sboros, and Meng-Xing Tang, *Senior Member, IEEE*

***Abstract*— Contrast echocardiography (CE) ultrasound with microbubble contrast agents has significantly advanced our capability for assessment of cardiac function, including myocardium perfusion quantification. However, in standard CE techniques obtained with line by line scanning, the frame rate and image quality are limited. Recent research has shown significant frame-rate improvement in noncontrast cardiac imaging. In this work, we present and initially evaluate, both *in vitro* and *in vivo*, a high-frame-rate (HFR) CE imaging system using diverging waves and pulse inversion sequence. An imaging frame rate of 5500 frames/s before and 250 frames/s after compounding is achieved. A destruction-replenishment sequence has also been developed. The developed HFR CE is compared with standard CE *in vitro* on a phantom and then *in vivo* on a sheep heart. The image signal-to-noise ratio and contrast between the myocardium and the chamber are evaluated. The results show up to 13.4-dB improvement in contrast for HFR CE over standard CE when compared at the same display frame rate even when the average spatial acoustic pressure in HFR CE is 36% lower than the standard CE. It is also found that when coherent compounding is used, the HFR CE image intensity can be significantly modulated by the flow motion in the chamber.**

***Index Terms*— Contrast-enhanced ultrasound (CEUS) imaging, high-frame-rate echocardiography, *in vivo*, myocardium perfusion, ultrafast diverging beams.**

I. Introduction

MICROBUBBLES for contrast-enhanced ultrasound (CEUS) imaging are bringing new information in clinical practice and preclinical research [1]. These microbubbles, or ultrasound contrast agents (UCAs), typically have a similar size (of the order of microns) to red blood cells with a gas core encapsulated by a phospholipid, albumin, or polymer shell. These bubbles are highly sensitive to ultrasound, thanks to their radial oscillations and resonant behavior, and once introduced into the blood stream intravenously, they can generate significant signal enhancement. Various signal processing techniques have been developed in order to achieve sensitive, specific, and quantitative imaging of UCA for flow and perfusion imaging [2], [3]. CEUS has shown great potential in the diagnosis and management of a range of cardiovascular diseases and cancer, and is gaining increasing acceptance clinically [1], [4]. Furthermore, the shells of the bubbles can be functionalized to target-specific molecule(s) of interest on the vascular endothelial wall, achieving ultrasound targeted/molecular imaging [4]. More recently, CEUS using low concentration of microbubbles, combined with localization of spatially isolated microbubbles, has been able to achieve subwavelength structural imaging of microvessels [5], [6].

Another significant advance in biomedical ultrasound is the development of high-frame-rate (HFR) US imaging techniques [7]. HFR US, with parallel data acquisition and digital beamforming, enables a frame rate of up to tens of thousands of images per second and offers exciting opportunities for US imaging. Indeed, recently HFR US has been applied to track fast shear waves in soft tissue elastography [8], [9], cardiac ultrafast 3-D Doppler imaging [10], cardiac strain imaging [11], blood flow velocity mapping [12], and brain functional imaging [6].

HFR CEUS, which combines CEUS with HFR US, can take advantage of both techniques and offer a unique opportunity for extracting new clinical information with improved US imaging capability. This is an exciting new area of research, and only a limited number of initial studies have been reported using clinical high-frequency linear probes on noncardiac applications. In [13] and [14], HFR CEUS has been shown to significantly expand the capability of existing nonlinear Doppler techniques in imaging both flow and perfusion from limited field of view to the full field of view. Couture and his colleagues have observed *in vitro* reduced bubble destruction [15] and improved imaging contrast [16] in HFR CEUS compared to the focused approach. We have demonstrated that HFR CEUS using plane wave transmission, combined with spatial and temporal signal processing, is able to produce

Manuscript received November 3, 2017; accepted July 12, 2018. Date of publication July 17, 2018; date of current version December 20, 2018. This work was supported by the Engineering and Physical Sciences Research Council under Grant EP/M011933/1 and Grant EP/M010961/1. *(Corresponding author: Matthieu Toulemonde.)*

M. Toulemonde, Y. Li, S. Lin, F. Cordonnier, and M.-X. Tang are with the Ultrasound Laboratory for Imaging and Sensing, Department of Bioengineering, Imperial College London, London SW7 2AZ, U.K. (e-mail: m.toulemonde@imperial.ac.uk; mengxing.tang@imperial.ac.uk).

M. Butler and V. Sboros are with the Institute of Biological Chemistry Biophysics and Bioengineering, Heriot-Watt University, Edinburgh EH14 4AS, U.K.

W. C. Duncan is with the MRC Center for Reproductive Health, The University of Edinburgh, Edinburgh EH16 4TJ, U.K.

R. J. Eckersley is with the Biomedical Engineering Department, Division of Imaging Sciences, King's College London, London SE1 7EH, U.K.

Digital Object Identifier 10.1109/TUFFC.2018.2856756

significantly improved vascular images *in vivo* [17]. Similar results have been observed by evaluating the impact of the flow velocity on the coherent compounding of plane wave amplitude modulation transmission [18]. We have recently demonstrated the use of HFR CEUS and image tracking for ultrasound imaging velocimetry (also called echo-particle imaging velocimetry) to map arterial flow and wall shear stress [19] and in visualizing the flow profile by controlled destruction of a volume of bubbles and observing the resulting bubble void subsequently evolve within the flow using HRF CEUS [20]. More recently, ultrasound superresolution of a rat brain has been demonstrated using HFR CEUS [6].

Non-HFR contrast echocardiography (CE) techniques have been developed [21] and extensively evaluated clinically [22] for myocardium perfusion quantification, thanks to the sensitivity offered by UCA. The ability to visualize and quantify perfusion defects in the myocardium is valuable for both diagnosis and treatment monitoring of, e.g., coronary artery disease. Typically, a relatively high amplitude ultrasound pulse is used to disrupt UCA within the imaging plane, followed by low-amplitude ultrasound pulses for monitoring replenishment of flow within the tissue. However, the key challenges in perfusion measurement are image quality. As reported in [23], physicians must become familiar with the criteria of an adequate contrast echocardiogram as well of artifacts to obtain the best contrast for left ventricular (LV) and myocardial opacification for myocardium perfusion assessment. Otherwise, it makes the technique highly operator dependent and limits its use. On the other hand, CE is routinely used clinically for significantly improved delineation and tracking of endocardium boundary in the LV, which compared to conventional ultrasound has shown to significantly increase the accuracy of the measurement of ejection fraction [23], [24]. The understanding of blood flow patterns within the heart chambers remains an under investigated area, however, which may provide additional heart function information [23], [25], [26]. This may partly be attributed to the inadequate temporal information and field of view that conventional CE is able to capture [25], [26].

Furthermore, noncontrast-enhanced cardiac HFR US techniques have also been developed using multiline acquisition [27], multiline transmission [28], [29] and diverging wave transmission [9], [30]–[34]. Multiline acquisition is based on the transmission of a wider focus beam and the creation of several received lines from the same transmission. The multiline transmission approach is the simultaneous transmission of focused waves at the same time. It improves the frame rate of the standard focused transmission by the number of multitransmissions. The best result is obtained by transmitting four focused transmissions at the same time and may also be used for tissue Doppler imaging [29], [35]. Diverging transmission is the successive transmission of unfocussed ultrasound waves using a virtual point source behind the probe and the coherent sum of the radio frequency (RF) images obtained in order to improve the image quality as in plane wave transmission [8], [31]. Diverging transmission has been used for tissue Doppler (250 frames/s) and vortography with motion correction [33], [34], Doppler imaging of the left ventricle (4800 frames/s) [32], and shear wave elastography by combining diverging transmission with pulse inversion (PI) ($>$1500 frames/s) [9]. Two kinds of diverging transmission have been proposed. In [9] and [31], the diverging waves are obtained by using a subaperture of the probe and the virtual source is placed at the center of the subaperture. Then, the subaperture is shifted a few elements, and this operation is repeated spanning along the length of the probe. In [9], [30], and [32]–[34], diverging waves are still obtained with a virtual point source but with the full aperture of the probe. The virtual source is moved behind the probe in order to create different diverging waves.

In [11], an overview of cardiac noncontrast-enhanced HFR US is given, including B-mode imaging improvement [28], [30], Doppler for tissue and LV imaging [32]–[34], [35] or blood flow dynamics in the myocardium using plane wave ultrafast Doppler imaging [36], neonatal hearts flow patterns tracking using speckle tracking [37], and motion and deformation imaging, shear waves, and tissue velocities calculation [9], [31]. Usually, these methods are implemented during postprocessing due to the high calculation power required. However, new echography research scanner are now capable to process calculations for vector Doppler and plane waves imaging in real time for a fastest interpretation [38].

The noncontrast-enhanced techniques presented above do not have as good a sensitivity to blood flow as that of CEUS, and it is very difficult if not impossible to use them to image myocardium perfusion. A further problem of noncontrast-enhanced cardiac HFR US is the difficulty in achieving similar levels of acoustic pressure at depth due to the lack of focusing during transmission.

Here, we present and initially evaluate both *in vitro* and *in vivo* an HFR CEUS system for imaging cardiac structure and flow and myocardium perfusion; following a recent preliminary study, we have reported at the IUS 2016 conference and a letter demonstrating the feasibility in-human [39], [40]. Compared to the in-human demonstration study, this study offers an in-depth description of the technical methodology, and a comprehensive evaluation of the techniques compared with traditional CE. The technique takes advantage of both UCA and HFR US, promising unprecedented imaging contrast and signal-to-noise ratio.

II. Materials and Methods

An HFR CE system based on a 128-Verasonics platform (Verasonics Inc., Redmond, WA) mounted a phased-array transducer (ATL P4-1, Phillips, Seattle, Washington) having 96 elements with a pitch of 295 μm and a central frequency of 2.5 MHz was developed. Performance was initially evaluated on both an *in vitro* phantom and *in vivo*.

A. Ultrasound Transmission Sequences

Three transmissions based on high-frame-rate imaging and classic line-by-line scanning approach were designed: HFR CE transmission, conventional CE transmission, and UCA destruction transmission.

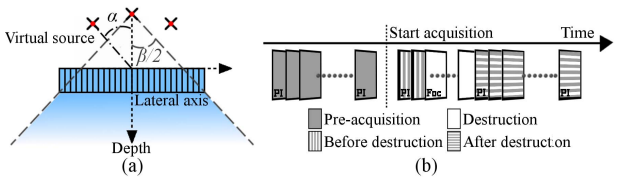

Fig. 1. (a) HFR CE angle transmission and (b) transmission sequence for real-time display and destruction-replenishment acquisition *in vitro* and *in vivo*.

1) High-Frame-Rate Contrast Echocardiography Transmission: The HFR CE imaging proposed here is defined by the coherent sum of PI diverging waves. Each diverging wave was obtained by defining a virtual source located behind the transducer to cover a large illumination area. The distance of the virtual source was linked to the full aperture and to an angular tilt angle α and width β which were defined by [33] and illustrated in Fig. 1(a). The angular tilt α defines the angle step of each compounding angles while β corresponds to the area illuminated.

In order to obtain a compounded image, the tilt angle α was varied while the angular width β was set constant. A 90° angular width was chosen corresponding to the angular aperture of the phase array probe. For each angle, two successive pulses in opposite phase were transmitted, recorded, and combined in postprocessing to form the PI image. Moreover, because of a possible nonperfect cancellation of the fundamental component due to the movement, a high pass zero-phase fifth-order Butterworth filter with a cutoff frequency at 2.7 MHz was used in order to extract the second-harmonic signal of the PI

2) Conventional Contrast Echocardiography Transmission: The CE transmission used corresponds to the CE imaging used in most existing ultrasound scanners: line-by-line scanning. CE transmission is combined to the MLA beamforming approach to reconstruct several lines simultaneously for each transmit pulse [27]. One CE image is obtained after the successive transmission of focused waves along an angular width (i.e., 90°). For each angle step, two low amplitude pulses in opposite phase are successively transmitted, recorded, and results combined to form the PI image. The same filter as HFR CE was used to extract the second-harmonic signal from PI images. The frame rate achieved was 30 Hz for a depth of 13 cm.

3) UCA Destruction Transmission: The UCA destruction, commonly used for measuring tissue blood replenishment (clinically termed "destruction-replenishment" or "destruction-reperfusion" method), is achieved by transmitting a focused 21-cycle burst signal of high intensity. While still well within the safety limit for ultrasound imaging, such a transmission is designed to destroy the UCA in the region of interest (ROI), i.e., the myocardium, and then allow the capture of replenishment of UCA within the same ROI.

4) Transmission Sequence Description: Two imaging transmission sequences are created, by combining destruction transmission with either HFR CE transmission or classic CE transmission, with a common timing as shown in Fig. 1(b). The preacquisition display, before and after destruction sequences correspond to either the classic CE or HFR CE. Before the destruction of the UCA, several frames are saved in order to compare the intensity before and after the destruction. Only the before destruction acquisition was used for *in vitro* experiments as the phantom was not dynamic, while the full sequences were used for *in vivo* experiments. Transmission parameters for both experiments are given in Table I. In order to achieve a frame rate of 30 Hz, CE transmission has an angle step of 1.1° which is not optimal for contrast imaging. Thus, MLA beamforming is processed to double the line density. The peak negative pressure as a function of depth of CE and HFR CE transmission is shown in Fig. 2. The peaks negative pressure of the sequences was measured in water using a calibrated hydrophone (Precision Acoutisc) with a derating factor of 0.3-dB cm^{-1} MHz^{-1}. The same peak negative pressures at 80 mm, given in Table I and corresponding to the CE focus depth, have been used for *in vivo* and *in vitro* experiments. Fig. 2 also shows the corresponding areas used in order to calculate the ratio of average pressure between CE and HFR CE. The ratio is obtained by calculating the ratio of the integrals of each curve. The minimum and maximum depths for the integrals have been selected based on the position of the myocardium during the *in vivo* acquisitions. It highlights that each HFR CE transmission has 36% lower average peak-negative pressure compared to CE.

TABLE I

TRANSMISSIONS PARAMETERS USED DURING *In Vitro* AND *In Vivo* EXPERIMENTS

	HFR CE	CE	Destruction
Frequency (Cycles)	1.5 MHz (3)	1.5 MHz (3)	2.5 MHz (21)
Temporal window	Gaussian	Gaussian	---
Number of angles/lines	11 (x2 PI)	82 (x2 PI)	128
Angular tilt α	-15°: 3° :15°	-45°: 1.1° :45°	-45°: 0.7° :45°
Angular width β	90°	90°	90°
Focus	---	80 mm	80 mm
Transmit / Receive Apodization	Square / Square	Square / Square	Square / Square
Frames (*in-vitro* / *in-vivo*)	125 / 1000	15 / 120	--- / 10
Pulse repetition frequency	5500 Hz	5500 Hz	---
Frame rate	250 Hz	30 Hz	45 Hz
Peak negative pressure at 80 mm	35 kPa	140 kPa	640 kPa

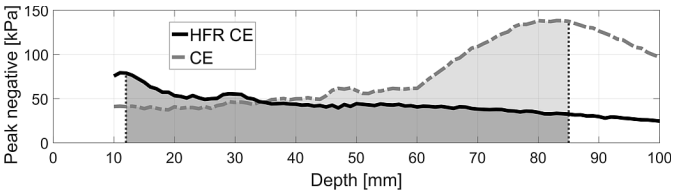

Fig. 2. Peak-negative pressure as a function of depth for HFR CE and CE and corresponding area for the ratio of average pressure between CE and HFR CE.

B. In Vitro Experimental Setup

A tissue mimicking phantom, consisting of polyvinyl alcohol (PVA) with a circular chamber, was developed for evaluating the HFR CE method. The center of the circular chamber is at 65 mm, and its diameter is about 30 mm. The tissue mimicking phantom was composed of (percentage of the total weight): PVA 10% (363146; Sigma-Aldrich), water 89%, and glass beads 1% (45–90 μm). The water was heated

at 90 °C, and PVA and glass beads were added slowly and cooked (with mixing) during 1 h. The mixture was left to cool at least 4 h for degasing. Then, three freeze–unfreeze cycles of 24 h each were realized [41]. The PVA phantom was then stored in a plastic box with water and detergent in a fridge. The 30 min before experiment, the phantom was removed from the fridge and washed and warmed. The phantom was set in a water tank filled with 20 L of water (24 °C) and 0.5 ml of Sonovue UCA (1/40 dilution) was mixed using a magnetic stirrer. All acquisitions lasted in total 6 min and during each transmission, the mixing was stopped.

C. In Vivo Sheep Heart Experimental Setup

The *in vivo* CE experiment was conducted under license from the U.K. Home Office at the University of Edinburgh, Edinburgh. The CE HFR was evaluated *in vivo* on an adult female Scottish Greyface sheep under terminal general anesthesia maintained using isofluorane [42]. The probe was held using a metallic arm in order to capture the same image of the left ventricle. The sheep was positioned slightly on the left side that ensured optimal heart imaging and avoided reflections from the ribs. During the acquisition, ventilation was transiently paused by extubation to avoid chest movement.

One conventional CE transmission and three HFR CE acquisitions were made on the same sheep with using one bolus injection of 1.2-mL Sonovue UCA followed by 7 mL of saline solution flush for each acquisition. The data acquisition, (baseline, destruction, and subsequent imaging) started 1 min after each bolus injection.

D. Postprocessing and Analysis

1) Image Postprocessing: In order to reduce noise and improve signal-to-noise ratio, an incoherently averaging in function of time of the HFR CE frames is applied in postprocessing. The frame rate of HFR CE is improved by a factor of 8 compared to the conventional CE.

Averaging seven envelope-detected HFR CE frames, with a triangular window centered on the interested frame, corresponds to a similar frame rate as the standard CE transmission. However, by doing an overlap time average, the same number of frames is obtained after the temporal filter. The image is named HFR CE SUM 7 in the figures while named SUM 7 in the paper.

2) Image Quality Evaluation: The image quality improvement is evaluated *in vitro* by measuring the contrast between the PVA tissue and the UCA and *in vivo* by measuring the contrast between the myocardium and UCA inside the chamber. The contrast evaluation is based on two equations: the contrast-to-acoustic-noise ratio (CANR) approach and the contrast-to-tissue (CTR) ratio. They are, respectively, defined as [43]–[45]

$$\mathrm{CANR} = \frac{|\mu_{\mathrm{ROI}} - \mu_{\mathrm{Tissue}}|}{\sqrt{\sigma^2_{\mathrm{ROI}} + \sigma^2_{\mathrm{Tissue}}}} \tag{1}$$

$$\mathrm{CTR} = 20\log_{10}\left(\frac{\mu_{\mathrm{ROI}}}{\mu_{\mathrm{Tissue}}}\right) \tag{2}$$

where in (1) μ_{ROI} and μ_{Tissue} are the mean in an ROI (usually a cyst) and the surrounding tissue. σ_{ROI} and σ_{Tissue} are their corresponding standard deviations. In (2), μ_{ROI} and μ_{Tissue} are the backscattered signals of the UCA and tissue, respectively.

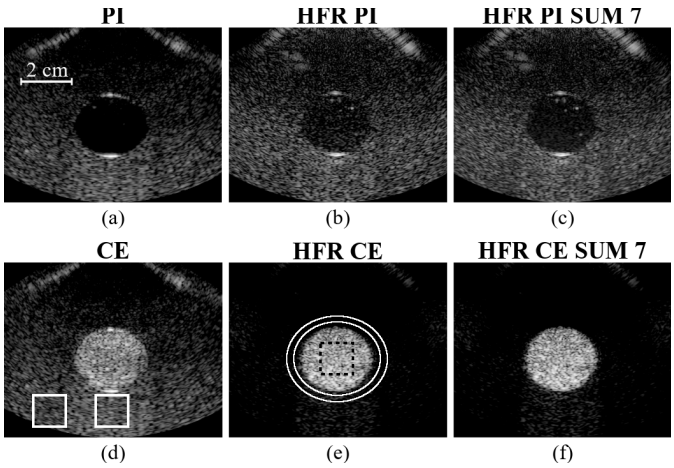

Fig. 3. PI images (a)–(c) without and (d)–(f) with microbubbles in the circular chamber of the PVA phantom for focused (a) and (d) CE, (b) and (e) HFR CE, and (c) and (f) HFR CE SUM 7. The white boxes in (d) are used to evaluate the NWP through the UCA. The black dashed box and the area between the two white ellipses in (e) show the microbubbles and tissue ROIs used for calculating CANR and CTR, respectively. Each image is normalized by its own maximum intensity and displayed with a dynamic range of 40 dB. Images are displayed between 20 and 100 mm and the lateral axis cover 100 mm.

Both equations are used for data analysis. For *in vitro* data, the ROI corresponds to the black box in the circular chamber containing UCA and the tissue region is the area between the two white ellipses. For *in vivo* data, the ROI and the tissue correspond to the cardiac chamber containing UCA and the myocardium divided into different segments, respectively. The myocardium segmentation was obtained using a fully automatic myocardial segmentation based on random forests guided by shape model [46]. Then, the myocardium segmentation is divided into six segments in order to evaluate the contrast at several depths.

The effect of nonlinear wave propagation (NWP) in ultrasound contrast agent is also evaluated *in vitro* for both transmissions. The NWP effect is calculated such as

$$\mathrm{NWP} = (\mu_{\mathrm{Tissue\ Propagation}} - \mu_{\mathrm{UCA\ Propagation}}) \tag{3}$$

where $\mu_{\mathrm{Tissue\ Propagation}}$ and $\mu_{\mathrm{UCA\ Propagation}}$ are the mean intensity, at the same depth in the lower part of the tissue phantom, away and below the UCA area, respectively.

CANR, CTR, and NWP are calculated for each acquisition frame (Table I), and their corresponding mean and standard deviation are provided.

3) Analysis of Destruction-Replenishment Data: In vivo destruction-replenishment analysis was evaluated from the time-intensity curve (TIC), and it is measured by using the myocardium segmentation described previously. The TIC is fit using the lognormal model proposed in [47] allowing the quantification of the disruption replenishment.

III. Results

A. In Vitro Experimental Setup

Fig. 3 shows one frame of the PVA phantom for conventional (a) and (d) CE, (b) and (e) HFR CE, and (c) and (f) SUM 7 acquisition. The images in the top of Fig. 3 are

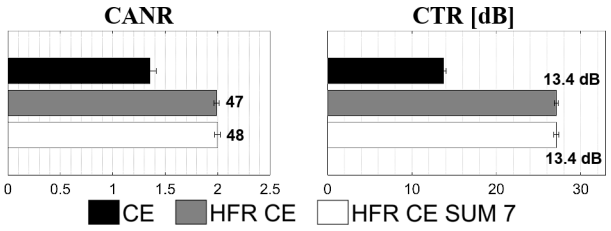

Fig. 4. CANR and CTR of the *in vitro* experiments calculated at several positions shown in Fig. 3(b). The bold values are the percentage or difference of improvement compared to the CE approach.

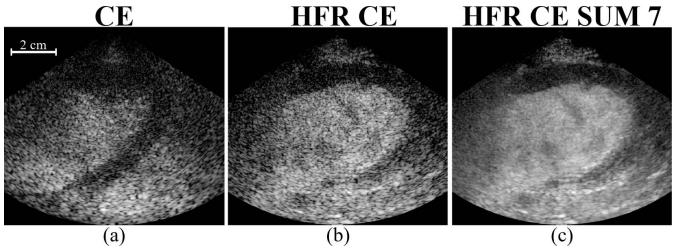

Fig. 5. (a) CE, (b) HFR CE (slow and fast frame rates), and (c) HFR CE SUM 7 (slow and fast frame rates) images of *in vivo* heart sheep experiments. CE and HFR CE are two successive acquisitions at the same position. All images are normalized and log compress by their own maximum and display with a dynamic range of 40 dB. The maximum depth is 90 mm and the lateral axis cover 100 mm.

without UCA while the images in the bottom are with UCA. Fig. 3(d) shows the areas where the NWP effect is evaluated, and Fig. 3(e) shows the UCA (black box) and tissue (zone between the two white ellipses) areas used for CANR and CTR evaluation.

With UCA, the contrast between the tissue and UCA is better for the HFR CE and SUM 7 than conventional CE. This is shown in Fig. 4, where CANR and CTR for the proposed HFR method are up to 48% and 13.4 dB higher than conventional CE method, respectively. For SUM 7, the CANR and CTR are similar to HFR CE because tissue and UCA are stationary, so the mean intensity and standard deviation vary similarly. The NWP effect calculated in the lower part of the phantom for CE, HFR CE, and HFR CE SUM7 is about 5.19 ± 0.15, 7.12 ± 0.28, and 6.74 ± 0.15 dB, respectively. It shows that the NWP effect is up to 1.48 dB higher for HFR CE than in CE transmission, reducing the contrast below the cyst area.

B. In Vivo Sheep Heart Experimental Setup

1) Evaluation of Image Quality: Fig. 5 shows one frame of the *in vivo* sheep acquisition for the conventional CE, HFR CE, and SUM 7 approaches. Five supplementary videos for Fig. 5 are available online. They correspond to the CE, HFR CE, and SUM 7 approaches. The HFR CE and SUM 7 videos are displayed in a slow and at a fast frame rate.

The central part of each image in Fig. 5 corresponds to the left ventricle which is filled with UCA. The darker area around the left ventricle is the myocardium. In conventional CE, the energy distribution is more concentrated at the focus (Fig. 2), improving the detection of the myocardium boundaries in this area compared to the top the myocardium which is not delineated as well as for the HFR CE approach. The visual delineation of the myocardium is improved by using temporal averaging filters in SUM 7.

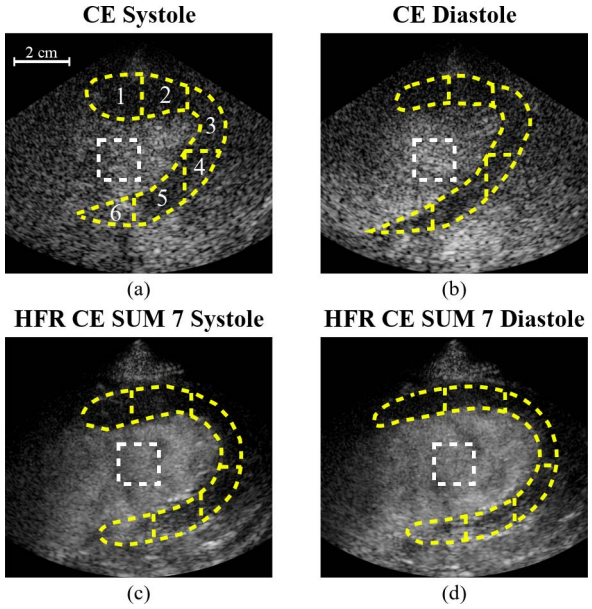

Fig. 6. (a) and (b) CE and (c) and (d) HFR CE SUM 7 images of *in vivo* heart sheep experiments at systole (left) and diastole (right). The white squares and yellow segments show the microbubble and myocardium areas used for CANR and CTR.

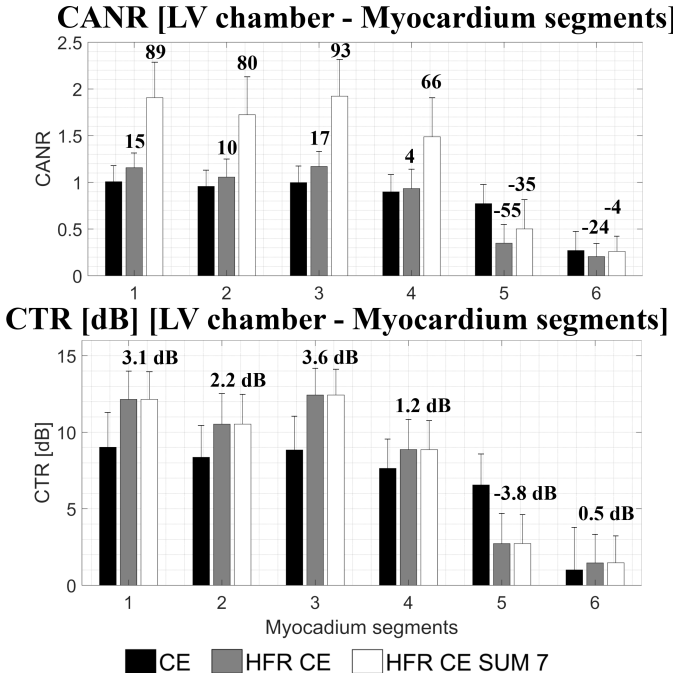

Fig. 7. CANR (top) and CTR (bottom) of the *in vivo* experiments calculated at several positions shown in Fig. 6. The bold values are the percentage of difference of improvement compared to the CE approach.

Fig. 6 shows the *in vivo* images with the myocardium segmentation obtained corresponding to the ROIs where the contrast between the myocardium and the chamber was evaluated. Two different phases of the heart cycle are provided (systole and diastole) in order to highlight the variation of the myocardium shape. The white squares and yellow segments show the microbubbles and myocardium areas used for CANR and CTR. The myocardium is divided into six segments, numbered in Fig. 6(a), and the corresponding quantification results are given in Fig. 7. The local peak negative pressure

TABLE II
LOCAL PEAK-NEGATIVE PRESSURE (P^-) AND MI AT THE DEPTH POSITION OF EACH *In Vivo* MYOCARDIUM SEGMENTS

		Segments					
		1	2	3	4	5	6
HFR CE	P^- (kPa)	53	49	45	42	41	35
	MI	*0.04*	*0.04*	*0.04*	*0.03*	*0.03*	*0.03*
CE	P^- (kPa)	39	39	46	61	75	113
	MI	*0.03*	*0.03*	*0.04*	*0.05*	*0.06*	*0.09*

and mechanical index (MI) corresponding to each segment for both transmission are given in Table II.

Fig. 7 shows that HFR CE improves the CANR and the CTR for the first fourth myocardium segments compared to the conventional CE. At the depth of the third segment, the MI of both transmissions is similar (Table II) and HFR CE is about 15% (1.2 dB) and 3.6 dB higher for CANR and CNR, respectively. In the lower ROI positions, the contrast is lower because it is close to the focus depth of the conventional CE with the highest local MI (Table II). Using temporal filter, the CANR in SUM7 is further improved for the first segments.

2) Destruction-Replenishment Analysis: Fig. 8 shows (left) the first HFR CE and HFR CE SUM 7 acquisition with their corresponding myocardium detection images at several times. The overall segmentation is used to evaluate their corresponding disruption-replenishment TIC, and there are shown in Fig. 8 (top right). Fig. 8 (bottom right) shows the three HFR CE disruption-replenishment TICs acquired successively and their corresponding lognormal fit.

The TIC normalized curves obtained for the HFC CE and SUM 7 have the same shape, even if SUM 7 is slightly smooth, as well as the lognormal curve fit. In the second TIC graph, the three HFR CE acquisitions look similar with a replenishment after the destruction of the microbubbles. Moreover, a regular sinusoidal pattern (every 0.53 s) is present corresponding to the heart cycle around 110 bpm.

IV. DISCUSSION

This paper presents *in vitro* and *in vivo* studies on HFR CE imaging methodology. It takes advantage of the high temporal resolution of HFR imaging and the high sensitivity of CEUS using ultrasound contrast agent, for imaging cardiac flow and myocardium perfusion. The main aim of this study is to evaluate any improvement in image quality and temporal resolution obtained for CE acquisition using diverging waves and PI approaches over existing focused transmission approaches.

The results from both *in vitro* and *in vivo* experiments show that compared to the existing standard focused CE process with two parallel beams in reception, HFR CE can generate higher CANR thanks to its higher imaging frame rate that allows using a combination of coherent and incoherent compounding.

While image resolution may decrease by the diverging wave imaging as there is no transmission focus, through multiangle transmission and beamforming with coherent compounding, focusing in both transmit and receive at every depth can be synthesized in HFR CE [30], [31]. In [33], an optimal HFR B-mode transmission combined to a motion estimation and correction has been proposed. In this proposed study, a tradeoff between grating lobes and frame rate has be made especially in contrast mode where twice more transmissions are required than B-mode imaging. A consecutive transmission of 11 ($\times 2$ PI) wide 90° diverging beam at 250 frames/s was chosen to acquire perfusion in all the myocardium after a microbubble destruction sequence.

The large amount of data acquired using HFR CE can be translated, thorough, e.g., compounding and averaging, too much superior CANR and CTR between UCA and tissue than conventional cardiac CE, for up to 48% (3.5 dB) and 13.4-dB improvement, respectively, *in vitro*, even when the spatial average peak negative pressure for the HFR CE is 36% lower than the standard CE. The increase in CTR and CANR for HFR CE in our results is likely due to the reduction of speckle (through compounding and averaging) that reduced the denominator of the CANR and potentially less nonlinear propagation of ultrasound in deep tissue due to its low peak negative pressure. However, the NWP evaluation shows that HFR CE has generated slightly more UCA signal than CE in the tissue even with a low concentration of UCA. One reason is that the CE focus point is slightly below the UCA area then less NWP is generated by the UCA. Another possibility is the low attenuation of the phantom (0.145 dB/MHz [41]) where second-harmonic signal is not attenuated as much as in cardiac tissue. As it has been investigated in [48] for CE acquisition, the NWP effect is the highest when the transmitted pulse is at the resonant frequency of the UCA. By reducing the MI or by using higher frequency, the NWP can be reduced but reducing the contrast. Further investigation for HFR CE transmission should be realized in order to optimize HFR CE transmission for lower NWP effect. *In vivo*, close to the probe where the local peak negative pressure of HFR CE is higher or close to CE (Table II), the CANR and CTR are improved up to 15% and 3.1 dB, respectively, but decrease near the focus area. Furthermore, thanks to the HFR of HFR CE, a temporal average, similar to a video filter, were applied by averaging seven weighted consecutives HFR CE envelope detected frames (so-called HFR CE SUM 7 or SUM 7) to achieve even further improvement without compromising the real-time display frame rate. Compared to CE, the CANR for HFR CE is improved up to 93% (5.7 dB) while CTR is not impacted by the smoothing effect. It should be noted that the CANR improvement for SUM7 is greater *in vivo* than that *in vitro*. This is likely due to the effect of temporal averaging in SUM7 which smooth more the *in vivo* chamber since the *in vitro* chamber did not have significant flow motion. The improvement in CTR *in vivo* is lower than *in vitro* because of the fast motion of the UCA in the chamber. Such fast motion reduces coherences between acquisitions from different steering angles and hence reduces the average image intensity in the chamber [19], [49].

The improvement for HFR CE over standard CE is despite of the unfavorable ultrasound pressure field for HFR CE, where the pressure in deep tissue for HFR CE is up to 4 times lower than that corresponding to an MI $= 0.1$ (Table II). In HFR diverging and plane wave CE, the acoustic pressure gradually decreases over depth, while in conventional CE with

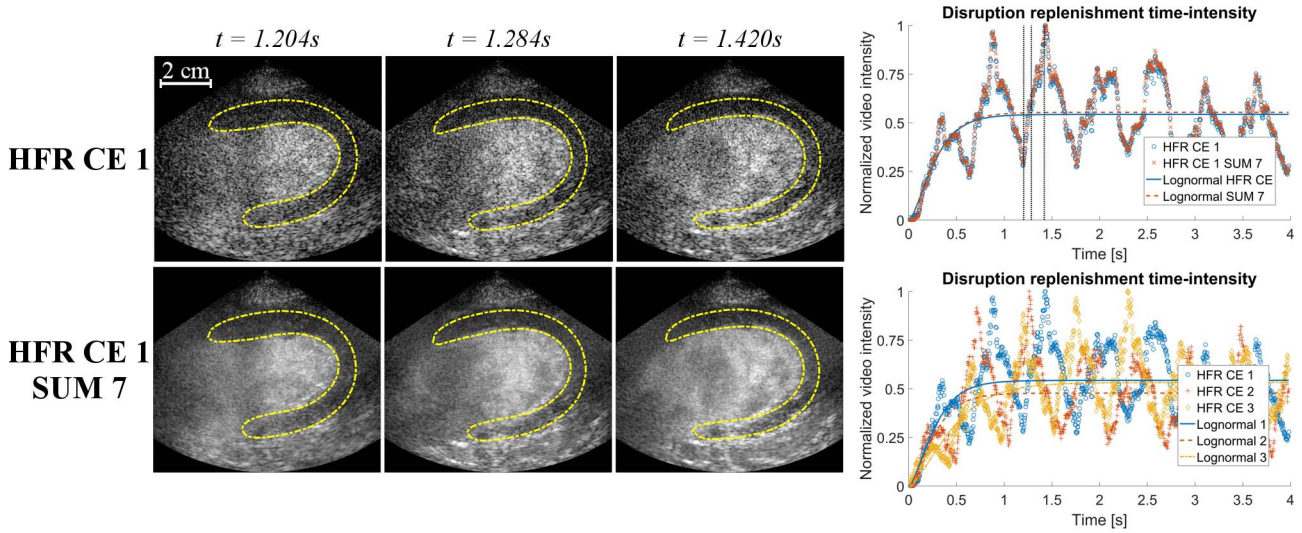

Fig. 8. HFR CE 1 and HFR CE SUM 7 myocardium detection images of *in vivo* experiments at several times (left) and TIC obtain for the corresponding HFR CE 1 and HFR CE SUM 7 myocardium detection shown on the left and the three different HFR CE acquisitions (right). All TICs are shown with their corresponding lognormal fit. The three dotted lines in the first TIC correspond to the time position of the HFR CE 1 and HFR CE SUM 7 images.

focused wave the pressure gradually increases toward the focus before decreasing again (Fig. 2). In this study, a low acoustic pressure/MI was used for HFR diverging CE. At the 80-mm CE focus depth, the acoustic peak-negative pressure for HFR CE is approximately 25% that of its focused counterpart. The highest peak-negative pressure in HFR CE, which is close to the transducer surface, is 79 kPa, corresponding to an MI of 0.06, compared to an MI of 0.11 in the focused CE sequence. Moreover, the ratio of average pressure between CE and HFR CE obtained the integral of each curves on Fig. 2, highlights that HFR CE has 36% lower average peak-negative pressure compared to CE for each transmission. Similar to plane wave CEUS imaging, a better contrast can be obtained with diverging and compounding acquisition [16], [18].

CANR is an image contrast measure to demonstrate the ability to distinguish echogenicity differences between two neighboring regions over noises (speckle and other noises). CANR $= 1$ means that the image intensity difference between the two regions is similar to the noise. Here, we use CANR to demonstrate the ability of different imaging techniques (CE versus HFR CE) to distinguish image intensity differences between contrast agent region and its neighboring tissue region over noises on phantom, and between the chamber and myocardium *in vivo*. It should be noted that the two lower parts of the myocardium (segments 5 and 6) in the *in vivo* results have CANRs lower than those of CE and much smaller than one, and it is difficult to distinguish the myocardium from the chamber. At these parts of the myocardium, the acoustic pressure of HFR CE is more than three times lower than that of CE.

It is noticeable that there are some patterns inside the chamber in Figs. 5 and 6. These are more noticeable in the SUM 7 image and in the supplementary videos provided online. Such patterns are absent in the conventional CE approach. The proposed HFR CE method is based on the coherent compounding of diverging waves, similar to the plane wave coherent

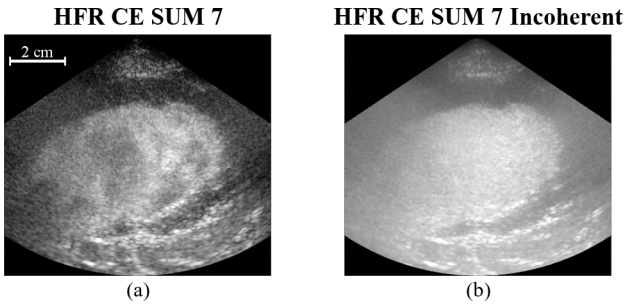

Fig. 9. (a) Coherent and (b) incoherent HFR CE SUM 7 images of *in vivo* heart sheep experiments. All images are normalized and log compress by their own maximum and display with a dynamic range of 40 dB. The maximum depth is 90 mm and the lateral axis cover is 100 mm.

compounding [8], [19]. Any presence of motion could induce a loss of signal coherence between compounding angles. If instead of coherent compounding, incoherent compounding is realized between all angles, the motion artifacts inside the chamber disappear because of the phase information lost. This approach is similar to spatial compounding for sector scan which has been investigated for standard focus transmission but suffered of low frame rate and a limited field of view [50]. Coherent and incoherent HFR CE SUM 7 compounding are shown in Fig. 9. A complementary video for Fig. 9 is available online corresponding to the incoherent HFR CE SUM 7 approach displayed in a fast frame rate. It is visible that motion artifacts are removed, and wall delineation and valves visualization are improved. The totally incoherent compounding has potential for chamber segmentation or valves visualization. However, this approach has some limits such as the image dynamic range which is significantly reduced, and some fine details inside the myocardium disappeared.

This loss of signal coherence between angles was analyzed for several UCA velocities in [18]. For HFR CE diverging transmission, 11 ($\times 2$ PI) angles are transmitted given a

compounded frame rate of 250 frames/s. Given the velocity of the myocardium which can reach a velocity of 9.4 $\text{cm} \cdot \text{s}^{-1}$ in the case of young healthy humans at rest [51], and the flow inside the chamber which can be higher than 1 $\text{m} \cdot \text{s}^{-1}$, there will be motion between the data acquisition during the multiple angle transmissions, and such motion could affect the final coherent sum, resulting in the image intensity being coded by flow velocity, in a sense similar to Doppler. This means that the quantification of image intensity in HFR CE varies with image settings. While there is motion compensation approach based on image registration can correct and improve the contrast-to-noise ratio [49], such patterns due to flow velocity may potentially hold clinical value for visualizing or even quantifying flow patterns within the chamber. Some clinical researches have investigated the vortex inside the heart for heart failure (204 ± 39 frames/s) or LV dysfunction (80 frames/s) by particle image velocimetry but was limited by the field of view and the frame-rate acquisition [25], [26]. The frame-rate improvement with the proposed method may improve the tracking of UCA for vortography especially during stress acquisition [25], [40], [52], [53]. Furthermore, the *in vivo* imaging protocol for HFR CE, including ultrasound parameters, is far from optimized. For instance, the number of compounding, the angle width, and the various angles defining the transmissions would significantly affect the final image quality specifically the segmentation of the deepest myocardium segments. These need further *in vivo* studies for optimization.

The *in vivo* experiment shows that the transmission sequence proposed with the Verasonics system scanner allows the quantification of myocardium perfusion by the destruction of the UCAs in the chamber and subsequent the acquisition of 1000 frames at 250 frames/s. The intensity inside the myocardium is low after the destruction of the UCA, and then it reaches a plateau as expected (Fig. 8). A recent random forest segmentation method is shown to be able to segment the HFR images and produce an oscillating pattern in the TIC curves corresponding to the heart rate of the sheep [46]. The lognormal fit is able to fit the TIC even if in the presence of this motion [47].

It should be noted that in the *in vivo* evaluation, the conventional CE and the HFR CE data were acquired on the same sheep heart but at different time points. This explains the slightly different shapes of the heart in the two acquisitions. It should also be noted that while HFR CE has successfully generated a TIC curve, the corresponding TIC curve of CE failed. While the better images obtained by HFR CE may have facilitated the generation of TIC, successful generation of TICs has been demonstrated by existing clinical systems that uses line-by-line scanning. The failure of generating TIC using CE may be due to the nonoptimized imaging parameters, and also the bolus injection used instead of constant infusion of microbubbles.

The HFR CE technique, by taking advantages of two most significant advances in ultrasound, i.e., HFR acquisition and UCA, is able to acquire a large amount of data from blood flow/perfusion with high sensitivity, without losing real-time frame rate. Such data would be able to either potentially reveal fast flow events not correctly visible using existing techniques, and/or significantly improve real-time image quality by combining data from multiple frames. This holds great potential in imaging cardiac flow and perfusion, by not only improving the existing applications such as myocardium perfusion quantification, but also potentially opening up new opportunities by visualizing fast/subtle features not discernable in existing techniques and improving wall delineation.

V. Conclusion

We have presented and initially evaluated a cardiac HFR CE imaging system. Initial evaluation has demonstrated that HFR CE generates superior image quality and has great potential to significantly improve the current cardiac imaging of flow and tissue perfusion.

Acknowledgment

The authors would like to thank Dr. V. Papadopoulou, Prof. R. Senior, and Prof. D. Cosgrove for their inputs in this study. They gratefully acknowledge the support of NVIDIA Corporation with the donation of the Titan Xp GPU used for this research.

References

[1] J. R. Lindner, "Microbubbles in medical imaging: Current applications and future directions," *Nature Rev. Drug Discovery*, vol. 3, pp. 527–533, Jun. 2004.

[2] A. Stanziola, M. Toulemonde, Y. O. Yildiz, R. J. Eckersley, and M.-X. Tang, "Ultrasound imaging with microbubbles [life sciences]," *IEEE Signal Process. Mag.*, vol. 33, no. 2, pp. 111–117, Mar. 2016.

[3] M.-X. Tang *et al.*, "Quantitative contrast-enhanced ultrasound imaging: A review of sources of variability," *Interface Focus*, vol. 1, no. 4, pp. 520–539, 2011.

[4] F. S. Villanueva and W. R. Wagner, "Ultrasound molecular imaging of cardiovascular disease," *Nature Clin. Pract. Cardiovascular Med.*, vol. 5, pp. S26–S32, Aug. 2008.

[5] K. Christensen-Jeffries, R. J. Browning, M.-X. Tang, C. Dunsby, and R. J. Eckersley, "*In vivo* acoustic super-resolution and super-resolved velocity mapping using microbubbles," *IEEE Trans. Med. Imag.*, vol. 34, no. 2, pp. 433–440, Feb. 2015.

[6] C. Errico *et al.*, "Ultrafast ultrasound localization microscopy for deep super-resolution vascular imaging," *Nature*, vol. 527, no. 7579, pp. 499–502, Nov. 2015.

[7] M. Tanter and M. Fink, "Ultrafast imaging in biomedical ultrasound," *IEEE Trans. Ultrason., Ferroelectr., Freq. Control*, vol. 61, no. 1, pp. 102–119, Jan. 2014.

[8] G. Montaldo, M. Tanter, J. Bercoff, N. Benech, and M. Fink, "Coherent plane-wave compounding for very high frame rate ultrasonography and transient elastography," *IEEE Trans. Ultrason., Ferroelectr., Freq. Control*, vol. 56, no. 3, pp. 489–506, Mar. 2009.

[9] M. Correia, J. Provost, S. Chatelin, O. Villemain, M. Tanter, and M. Pernot, "Ultrafast harmonic coherent compound (UHCC) imaging for high frame rate echocardiography and shear-wave elastography," *IEEE Trans. Ultrason., Ferroelectr., Freq. Control*, vol. 63, no. 3, pp. 420–431, Mar. 2016.

[10] J. Provost *et al.*, "3D ultrafast ultrasound imaging *in vivo*," *Phys. Med. Biol.*, vol. 59, no. 19, pp. L1–L13, 2014.

[11] M. Cikes, L. Tong, G. R. Sutherland, and J. D'hooge, "Ultrafast cardiac ultrasound imaging technical principles, applications, and clinical benefits," *JACC, Cardiovascular Imag.*, vol. 7, no. 8, pp. 812–823, 2014.

[12] B. Y. S. Yiu, S. S. M. Lai, and A. C. H. Yu, "Vector projectile imaging: Time-resolved dynamic visualization of complex flow patterns," *Ultrasound Med. Biol.*, vol. 40, no. 9, pp. 2295–2309, Sep. 2014.

[13] C. Tremblay-Darveau, R. Williams, L. Milot, M. Bruce, and P. N. Burns, "Combined perfusion and Doppler imaging using plane-wave nonlinear detection and microbubble contrast agents," *IEEE Trans. Ultrason., Ferroelectr., Freq. Control*, vol. 61, no. 12, pp. 1988–2000, Dec. 2014.

[14] C. Tremblay-Darveau, R. Williams, L. Milot, M. Bruce, and P. N. Burns, "Visualizing the tumor microvasculature with a nonlinear plane-wave Doppler imaging scheme based on amplitude modulation," *IEEE Trans. Med. Imag.*, vol. 35, no. 2, pp. 699–709, Feb. 2016.

[15] O. Couture, S. Bannouf, G. Montaldo, J. F. Aubry, M. Fink, and M. Tanter, "Ultrafast imaging of ultrasound contrast agents," *Ultrasound Med. Biol.*, vol. 35, no. 11, pp. 1908–1916, 2009.

[16] O. Couture, M. Fink, and M. Tanter, "Ultrasound contrast plane wave imaging," *IEEE Trans. Ultrason., Ferroelectr., Freq. Control*, vol. 59, no. 12, pp. 2676–2683, Dec. 2012.

[17] A. Stanziola, C. H. Leow, E. Bazigou, P. D. Weinberg, and M. X. Tang, "ASAP: Super-contrast vasculature imaging using coherence analysis and high frame- rate contrast enhanced ultrasound," *IEEE Trans. Med. Imag.*, to be published, doi: 10.1109/TMI.2018.2798158.

[18] J. Viti, H. J. Vos, N. de Jong, F. Guidi, and P. Tortoli, "Detection of contrast agents: Plane wave versus focused transmission," *IEEE Trans. Ultrason. Ferroelectr., Freq. Control*, vol. 63, no. 2, pp. 203–211, Feb. 2016.

[19] C. H. Leow and M. X. Tang, "Spatio-temporal flow and wall shear stress mapping based on incoherent ensemble-correlation of ultrafast contrast enhanced ultrasound images," *Ultrasound Med. Biol.*, vol. 44, no. 1, pp. 134–152, 2018.

[20] C. H. Leow *et al.*, "Microbubble void imaging: A non-invasive technique for flow visualisation and quantification of mixing in large vessels using plane wave ultrasound and controlled microbubble contrast agent destruction," *Ultrasound Med. Biol.*, vol. 41, no. 11, pp. 2926–2937, 2015.

[21] K. Wei, A. R. Jayaweera, S. Firoozan, A. Linka, D. M. Skyba, and S. Kaul, "Quantification of myocardial blood flow with ultrasound-induced destruction of microbubbles administered as a constant venous infusion," *Circulation*, vol. 97, pp. 473–483, Feb. 1998.

[22] R. Senior *et al.*, "Comparison of sulfur hexafluoride microbubble (SonoVue)-enhanced myocardial contrast echocardiography with gated single-photon emission computed tomography for detection of significant coronary artery disease: A large European multicenter study," *J. Amer. College Cardiol.*, vol. 62, no. 15, pp. 1353–1361, 2013.

[23] R. Senior *et al.*, "Clinical practice of contrast echocardiography: Recommendation by the European association of cardiovascular imaging (EACVI)," *Eur. Heart J.-Cardiovascular Imag.*, vol. 18, no. 11, p. 1205af, 2017.

[24] T. R. Porter *et al.*, "Clinical applications of ultrasonic enhancing agents in echocardiography: 2018 American society of echocardiography guidelines update," *J. Amer. Soc. Echocardiography*, vol. 31, no. 3, pp. 241–274, 2018.

[25] H. Abe *et al.*, "Contrast echocardiography for assessing left ventricular vortex strength in heart failure: A prospective cohort study," *Eur. Heart J.-Cardiovascular Imag.*, vol. 14, no. 11, pp. 1049–1060, 2012.

[26] L. Agati *et al.*, "Quantitative analysis of intraventricular blood flow dynamics by echocardiographic particle image velocimetry in patients with acute myocardial infarction at different stages of left ventricular dysfunction," *Eur. Heart J.-Cardiovascular Imag.*, vol. 15, no. 11, pp. 1203–1212, 2014.

[27] D. P. Shattuck, M. D. Weinshenker, S. W. Smith, and O. T. von Ramm, "Explososcan: A parallel processing technique for high speed ultrasound imaging with linear phased arrays," *J. Acoust. Soc. Amer.*, vol. 75, no. 4, pp. 1273–1282, 1984.

[28] L. Tong, H. Gao, H. F. Choi, and J. D'hooge, "Comparison of conventional parallel beamforming with plane wave and diverging wave imaging for cardiac applications: A simulation study," *IEEE Trans. Ultrason., Ferroelectr., Freq. Control*, vol. 59, no. 8, pp. 1654–1663, Aug. 2012.

[29] L. Tong, A. Ramalli, R. Jasaityte, P. Tortoli, and J. D'hooge, "Multi-transmit beam forming for fast cardiac imaging—Experimental validation and *in vivo* application," *IEEE Trans. Med. Imag.*, vol. 33, no. 6, pp. 1205–1219, Jun. 2014.

[30] H. Hasegawa and H. Kanai, "High-frame-rate echocardiography using diverging transmit beams and parallel receive beamforming," *J. Med. Ultrason.*, vol. 38, no. 3, pp. 129–140, 2011.

[31] C. Papadacci, M. Pernot, M. Couade, M. Fink, and M. Tanter, "High-contrast ultrafast imaging of the heart," *IEEE Trans. Ultrason., Ferroelectr., Freq. Control*, vol. 61, no. 2, pp. 288–301, Feb. 2014.

[32] B.-F. Osmanski, D. Maresca, E. Messas, M. Tanter, and M. Pernot, "Transthoracic ultrafast Doppler imaging of human left ventricular hemodynamic function," *IEEE Trans. Ultrason., Ferroelectr., Freq. Control*, vol. 61, no. 8, pp. 1268–1275, Aug. 2014.

[33] J. Porée, D. Posada, A. Hodzic, F. Tournoux, G. Cloutier, and D. Garcia, "High-frame-rate echocardiography using coherent compounding with Doppler-based motion-compensation," *IEEE Trans. Med. Imag.*, vol. 35, no. 7, pp. 1647–1657, Jul. 2016.

[34] J. Faurie *et al.*, "Intracardiac vortex dynamics by high-frame-rate Doppler vortography—*In vivo* comparison with vector flow mapping and 4-D flow MRI," *IEEE Trans. Ultrason., Ferroelectr., Freq. Control*, vol. 64, no. 2, pp. 424–432, Feb. 2017.

[35] L. Tong *et al.*, "hooge, "Wide-angle tissue Doppler imaging at high frame rate using multi-line transmit beamforming: An experimental validation *in vivo*," *IEEE Trans. Med. Imag.*, vol. 35, no. 2, pp. 521–528, Feb. 2016.

[36] B. F. Osmanski, M. Pernot, G. Montaldo, A. Bel, E. Messas, and M. Tanter, "Ultrafast Doppler imaging of blood flow dynamics in the myocardium," *IEEE Trans. Med. Imag.*, vol. 31, no. 8, pp. 1661–1668, Aug. 2012.

[37] S. Fadnes, S. A. Nyrnes, H. Torp, and L. Lovstakken, "*In vivo* intracardiac vector flow imaging using phased array transducers for pediatric cardiology," *IEEE Trans. Ultrason., Ferroelectr., Freq. Control*, vol. 64, no. 9, pp. 1318–1326, Sep. 2017.

[38] S. Ricci, L. Bassi, and P. Tortoli, "Real-time vector velocity assessment through multigate Doppler and plane waves," *IEEE Trans. Ultrason., Ferroelectr., Freq. Control*, vol. 61, no. 2, pp. 314–324, Feb. 2014.

[39] M. Toulemonde *et al.*, "Cardiac imaging with high frame rate contrast enhanced ultrasound: *In-vivo* demonstration," in *Proc. IEEE Int. Ultrason. Symp.*, Tours, France, Sep. 2016, pp. 1–4.

[40] M. E. G. Toulemonde *et al.*, "High frame-rate contrast echocardiography: In-human demonstration," *JACC, Cardiovascular Imag.*, vol. 11, no. 6, pp. 923–924, 2018.

[41] A. J. Y. Chee, C. K. Ho, B. Y. S. Yiu, and A. C. H. Yu, "Walled carotid bifurcation phantoms for imaging investigations of vessel wall motion and blood flow dynamics," *IEEE Trans. Ultrason., Ferroelectr., Freq. Control*, vol. 63, no. 11, pp. 1852–1864, Nov. 2016.

[42] F. Connolly *et al.*, "The local effects of ovarian diathermy in an ovine model of polycystic ovary syndrome," *PLoS ONE*, vol. 9, no. 10, p. e111280, 2014.

[43] J. M. Thijssen, "Ultrasonic speckle formation, analysis and processing applied to tissue characterization," *Pattern Recognit. Lett.*, vol. 24, nos. 4–5, pp. 659–675, Feb. 2003.

[44] A. C. Jensen, S. P. Nasholm, C.-I. C. Nilsen, A. Austeng, and S. Holm, "Applying Thomson's multitaper approach to reduce speckle in medical ultrasound imaging," *IEEE Trans. Ultrason., Ferroelectr., Freq. Control*, vol. 59, no. 10, pp. 2178–2185, Oct. 2012.

[45] F. Lin, C. Cachard, F. Varray, and O. Basset, "Generalization of multipulse transmission techniques for ultrasound imaging," *Ultrason. Imag.*, vol. 37, no. 4, pp. 294–311, 2015.

[46] Y. Li, C. P. Ho, M. Toulemonde, N. Chahal, R. Senior, and M.-X. Tang, "Fully automatic myocardial segmentation of contrast echocardiography sequence using random forests guided by shape model," *IEEE Trans. Med. Imag.*, vol. 37, no. 5, pp. 1081–1091, May 2018.

[47] J. M. Hudson, R. Karshafian, and P. N. Burns, "Quantification of flow using ultrasound and microbubbles: A disruption replenishment model based on physical principles," *Ultrasound Med. Biol.*, vol. 35, no. 12, pp. 2007–2020, Dec. 2009.

[48] M.-X. Tang, N. Kamiyama, and R. J. Eckersley, "Effects of nonlinear propagation in ultrasound contrast agent imaging," *Ultrasound Med. Biol.*, vol. 36, no. 3, pp. 459–466, Mar. 2010.

[49] M. Toulemonde *et al.*, "Effects of motion on high frame rate contrast enhanced echocardiography and its correction," in *Proc. IEEE Int. Ultrason. Symp.*, Washington, DC, USA, Sep. 2017, pp. 1–4.

[50] D. P. Shattuck and O. T. von Ramm, "Compound scanning with a phased array," *Ultrason. Imag.*, vol. 4, no. 2, pp. 93–107, 1982.

[51] A. Thorstensen, H. Dalen, B. H. Amundsen, and A. Støylen, "Peak systolic velocity indices are more sensitive than end-systolic indices in detecting contraction changes assessed by echocardiography in young healthy humans," *Eur. J. Echocardiography*, vol. 12, no. 12, pp. 924–930, 2011.

[52] M. Toulemonde *et al.*, "Cardiac flow mapping using high frame rate diverging wave contrast enhanced ultrasound and image tracking," in *Proc. IEEE Int. Ultrason. Symp.*, Washington, DC, USA, Sep. 2017, pp. 1–4.

[53] J. Voorneveld *et al.*, "High frame rate ultrasound particle image velocimetry for estimating high velocity flow patterns in the left ventricle," *IEEE Trans. Ultrason., Ferroelectr., Freq. Control*, to be published, doi: 10.1109/TUFFC.2017.2786340.

Matthieu Toulemonde (S'12–A'14–M'17) was born in Béziers, France, in 1988. He received the bachelor's degree in physics and chemistry and the master's degree in optics, image and signal processing from l'Université Jean Monnet de Saint-Étienne, Saint-Étienne, France, in 2009 and 2011, respectively, and the Ph.D. degree from l'Université Lyon 1, Lyon, France, and Università degli Studi di Florence, Florence, Italy, in 2014, with a focus on beamforming and nonlinearity parameter estimation.

His Ph.D. research was realized in co-agreement between the Centre de Recherche en Acquisition et Traitement de l'Image pour la Santé, Lyon, France, and the MSD Laboratory, Florence, Italy. Since 2015, he has been a Research Associate with the Ultrasound Laboratory for Imaging and Sensing, Imperial College London, London, U.K. His current research interests include contrast enhanced ultrasound, myocardium perfusion, and ultrafast cardiac imaging.

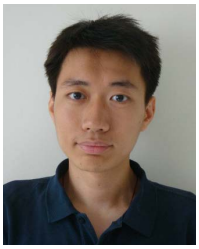

Yuanwei Li received the B.Eng. degree in biomedical engineering from Imperial College London, London, U.K., in 2012, the M.Sc. degree in computer science from the University of Oxford, Oxford, U.K., in 2013, and the Ph.D. degree in biomedical engineering from Imperial College London, London, in 2017.

He is currently a Post-Doctoral Researcher of medical image analysis with Imperial College London. His research interest includes medical image processing and analysis, computer vision, machine learning, image segmentation, and registration.

Dr. Li was a recipient of the Imperial College President's Ph.D. Scholarship.

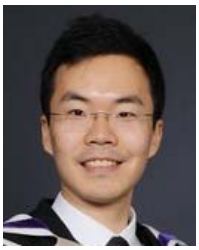

Shengtao Lin (GS'14) received the M.Sc. and Ph.D. degrees in biomedical engineering from the Ultrasound Laboratory for Imaging and Sensing Group, Department of Bioengineering, Imperial College London, London, U.K., under the supervision of Prof. M. Tang. His research interests include nanodroplet/microbubble contrast agents for photoacoustic and ultrasound imaging.

Fabien Cordonnier studied signal processing and data analysis with Ecole Centrale Nantes. He received the M.Sc. degree in biomedical engineering from Imperial College London. His master's thesis focused on the quantification of myocardial contrast echocardiograms for diagnosis of coronary artery disease.

He was an Intern at the Eriksholm Research Centre, focused on electroencephalogram analysis following auditory brain processing. He is currently a Data Analyst with Criteo, Paris, France, where he processes online marketing data and turns it into actionable insights, including performance reviews and opportunity forecasts.

Mairead Butler received the M.Phys. degree (Hons.) in physics from The University of Bath, Bath, U.K., in 2001, including an industrial placement at the Proudman Oceanographic Laboratory, Liverpool, U.K., from 2000 to 2001, and the Ph.D. degree in the medical physics section of The University of Edinburgh, Edinburgh, U.K., in 2006.

She was a Post-Doctoral Researcher of the Engineering and Physical Sciences Research Council and British Heart Foundation funded projects at the University of Edinburgh from 2004 to 2012, followed by the British Heart Foundation and Medical Research Council funded projects at Heriot-Watt University, Edinburgh. Her current research interests include imaging microvasculature structure using contrast-enhanced ultrasound.

W. Colin Duncan received the M.B.ChB. degree from the University of Edinburgh, Edinburgh, U.K., in 1990.

His research training included a Wellcome Trust Clinical Training Fellowship at the Medical Research Council Reproductive Biology Unit and a Clinician Scientist and Scottish Senior Clinical Fellowship at the University of Edinburgh. He is currently a Professor of reproductive medicine and science with the Medical Research Council Centre for Reproductive Health, University of Edinburgh. He runs a research laboratory that studies normal ovarian physiology and polycystic ovary syndrome and is interested in preclinical large animal research models. He is currently a fellow of the Royal College of Obstetricians and Gynaecologists, London, U.K., and works as a Clinician with the Edinburgh Fertility and Reproductive Endocrine Centre, Royal infirmary of Edinburgh, Edinburgh.

Robert J. Eckersley (M'98–SM'13) received the B.Sc. degree in physics from King's College London, London, U.K., in 1991, and the Ph.D. degree from the University of London in 1997 while studying at the Institute of Cancer Research, Royal Marsden Hospital, London.

He was with the Hammersmith Hospital NHS Trust and in 1999 was awarded an MRC Research Training Fellowship. As part of this fellowship, he spent some time at the University of Toronto, Sunnybrook Health Sciences Centre, Toronto, ON, Canada. He was a Post-Doctoral Researcher with the Imaging Sciences Department, Imperial College London, London, and became a nonclinical Lecturer of ultrasound in 2007. Since 2012, he has been a Senior Lecturer with the School of Biomedical Engineering and Imaging Sciences, King's College London. His research interests range from fundamental studies to clinical applications and include image and signal analysis of ultrasound data for improving imaging quality and quantitative measurement, nonlinear imaging for improved detection of microbubbles, and understanding errors and artifacts in ultrasound contrast imaging.

Vassilis Sboros was born in Volos, Greece, in 1968. He received the Degree in physics from the University of Athens, Athens, Greece, in 1993, the M.Sc. degree in medical physics from the University of Aberdeen, Aberdeen, U.K., in 1994, and the Ph.D. degree in ultrasound contrast imaging from The University of Edinburgh, Edinburgh, U.K., in 1999.

The jobs that followed investigated the physics of microbubbles and the engineering of imaging them. He has authored over 50 peer-reviewed papers. His current research interests include clinical and preclinical ultrasound imaging.

Meng-Xing Tang (M'05–SM'17) joined Imperial College London, London, U.K., as a Lecturer (Assistant Professor) in 2006, when founded what is now the Ultrasound Laboratory for Imaging and Sensing (previously known as the Ultrasound Imaging Group). He was promoted to Senior Lecturer in 2011 and Reader in 2015. He is currently a Reader (Associate Professor) of biomedical imaging with the Department of Bioengineering, Imperial College London. In the past years, his group has investigated extensively the imaging physics of microbubble contrast agents (MBs), the various imaging artifacts in CEUS and their correction methods, in order to achieve more reliable quantification of tissue perfusion. More recently, his group has been developing and applying new contrast-enhanced ultrasound imaging techniques of very high temporal and spatial resolution and image contrast. His research has been generously funded by U.K. EPSRC, Cancer Research U.K., the British Heart Foundation, the Wellcome Trust, and the Royal Society. He has authored over 80 peer-reviewed journal papers. His current research focuses on developing new imaging and image analysis techniques using ultrasound and its allied techniques, such as MBs, for quantifying physiological flow, tissue perfusion, and molecular information, and their applications in cardiovascular diseases, cancer, and neurology.

Dr. Tang is an Associate Editor of IEEE TRANSACTIONS ON ULTRASONICS, FERROELECTRICS, AND FREQUENCY CONTROL, and is on the Editorial Advisory Board of *Ultrasound in Medicine and Biology*.